Direct observation of the spatial and temporal dynamics of polaron diffusion in $SrTiO_3$

Kohmoto, T.
Ikeda, D.
Liang, X.
Moriyasu, T.

(Citation)
Physical Review B,87(21):214301-214301

(Issue Date)
2013-06-05

(Resource Type)
journal article

(Version)
Version of Record

PHYSICAL REVIEW B **87**, 214301 (2013)

Direct observation of the spatial and temporal dynamics of polaron diffusion in $SrTiO_3$

T. Kohmoto, D. Ikeda, X. Liang, and T. Moriyasu
Graduate School of Science, Kobe University, Kobe 657-8501, Japan
(Received 11 January 2013; published 5 June 2013)

The generation, relaxation, and diffusion dynamics of optically induced lattice distortion in the relaxed excited state of $SrTiO_3$ are studied by using polarization spectroscopy with the pump-probe technique. The relaxed excited state is generated with a rise time on the order of 100 ps. Three kinds of thermal activation processes of the localized lattice distortion are found, and these processes are considered to be caused by photogenerated carriers in trapped states, which play important roles in photoluminescence or photoconductivity. We observed the lattice distortion induced by a separated pump beam from the probe beam to investigate its itineracy. The lattice-distortion signal appears later as the separation along the [100] axis becomes larger. The temperature dependence of the mobility suggests that the observed diffusive lattice distortion is caused by photogenerated electrons accompanied by lattice distortion, or electron polarons. Thus, the spatial and temporal dynamics of polaron diffusion were observed directly in our experiment.

DOI: 10.1103/PhysRevB.87.214301 PACS number(s): 71.38.−k, 72.40.+w, 78.20.Fm, 78.47.D−

I. INTRODUCTION

Elementary excitations, such as phonons, magnons, polaritons, excitons, and polarons, are a mathematical tool for simplifying the description of solids. They are not real particles inside a solid but are most important in condensed matter physics, as they are one of the few known ways of simplifying the quantum mechanical many-body problem. A charge coupled with phonons in a crystal forms a quasiparticle called a polaron, which is composed of a charge and a phonon cloud around it. The charge moves through the crystal and carries the lattice distortion with it. The concept of a polaron[1,2] is essential to understand the physical properties of charge carriers in ionic crystals, semiconductors, and organic crystals.

The dynamics of polarons, such as their generation and relaxation, has been studied by the transient measurements of absorption,[3] reflection,[4] or photoconductivity.[5] Polarons are also expected to move diffusively in solids. However, the direct observation of polaron diffusion has not been reported so far, although indirect observations were discussed in the experiments of magnetic resonance.[6,7] In the present paper, we report the direct observation of the spatial and temporal dynamics of polaron diffusion in strontium titanate $SrTiO_3$.

$SrTiO_3$ is an insulator with a band gap of $\sim$3.2 eV and well known as an incipient ferroelectric material. In spite of the extremely large dielectric constant of $\sim 10^4$ and softening of the lowest TO phonon mode toward a ferroelectric transition, the paraelectric phase is stabilized, and the quantum paraelectric state is maintained down to 0.3 K.[8]

$SrTiO_3$ is also well known for high photoconductivity.[9,10] According to photo-Hall studies, most photocurrent carriers are negatively charged, with a mobility as high as 10^4 $cm^2/V\,s$ at liquid helium temperatures.[11,12] Their high mobility shown in the transport measurements is consistent with the photogenerated carriers whose localized character was discussed in the optical measurements.[9,13–15]

It has been found that the dielectric constant in $SrTiO_3$ is drastically enhanced by the weak UV illumination whose energy is larger than the optical band-gap energy of 3.2 eV.[16,17] This enhancement may be a kind of photoinduced structural phase transition,[18] and a coupling between photogenerated electrons and phonons, which forms polarons, is expected to play an important role in the enhancement. A possibility was discussed that a dramatic enhancement of the dielectric constant can be caused by a huge dipole moment of the polar domain,[17] and a theory of superparaelectric large polaron has been proposed.[19] Recently, the existence of excitonic effects in the optical absorption spectrum is also discussed.[20]

In the present paper, the generation and relaxation dynamics of optically induced lattice distortion in $SrTiO_3$ are studied by using polarization spectroscopy with the pump-probe technique. We observed the lattice distortion induced by a separated pump beam from the probe beam and show experimental evidence that the optically induced lattice distortion diffuses along the [100] axis.

II. EXPERIMENT

In our experiment, the pump pulse is provided by a Ti:sapphire regenerative amplifier (800 nm, 0.2 ps, $\sim$10 μJ, 250 Hz). The probe pulse from an optical parametric amplifier (700 nm, 0.2 ps) and an optical delay line are used for the experiment in the picosecond regime, and the probe light from a laser diode (660 nm, continuous wave) and a signal averager are used for the experiment in the millisecond regime. The directions of the linearly polarized pump and probe beams are collinear and perpendicular to the (001) surface of a sample in a temperature-controlled refrigerator, whose thickness is 0.2 mm. The beam diameter of the focused beams is $\sim$50 μm at the sample.

A lattice distortion is generated in the relaxed excited state by the pump pulse through a multiphoton absorption process, and a time-dependent anisotropy of the refractive index is induced. The induced anisotropy of the refractive index, or linear birefringence, is detected using a polarimeter[21] with a quarter-wave plate as the change in the polarization of the probe beam, where the polarization plane of the probe beam is tilted by 45° from that of the pump beam and the ellipticity of the transmitted probe beam caused by the birefringence is monitored.

III. GENERATION AND RELAXATION OF THE LATTICE-DISTORTION SIGNAL

The ultraviolet illumination, whose energy is larger than the $SrTiO_3$ band-gap energy of 3.2 eV, excites electrons from the ground state to the excited state. The photogenerated carriers are self-trapped in the relaxed excited state through charge-phonon interactions, where a lattice distortion is generated. This is an optically induced lattice distortion. In $SrTiO_3$, the electron-hole interaction is considered to be small because of the large dielectric constant, and the electrons and holes are considered to be self-trapped independently as polarons without exciton formation. The relaxed excited state disappears owing to the recombination of the carriers with luminescence.

The observed generation and relaxation signals of the lattice distortion are shown in Figs. 1(a) and 1(b), in which the polarization plane of the pump pulse is along the [100] axis. The vertical axis, which is plotted on a linear scale in Fig. 1(a) and on a logarithmic scale in Fig. 1(b), is the ellipticity of the transmitted probe beam owing to the transient birefringence after pulse excitation at $t = 0$. At low temperatures, the change in the probe polarization (ellipticity) generated by the optically induced lattice distortion is $\approx 10^{-3}$ in the electric field amplitude, which corresponds to the anisotropy in refractive index (birefringence) $\Delta n \approx 10^{-6}$. The rise time of the lattice-distortion signal in Fig. 1(a) is on the order of 100 ps, which is consistent with the rise time observed in the transient-absorption experiment.[22] These results show that it takes ~100 ps to generate the relaxed excited state.

The observed amplitude of the lattice distortion is found to depend on the square of the pump pulse energy as shown in our preliminary report.[23] The dependence of the amplitude on the pump pulse energy is shown in Fig. 1(c). This nonlinear behavior of the signal for the pulse energy suggests that the relaxed excited state is generated through a two-photon absorption process. The luminescence spectrum for this pulse excitation is almost the same as that for direct ultraviolet excitation.[22] The energy 3.10 eV of this two-photon absorption process is less than the band-gap energy 3.16 eV.[14] The strong electric field and broad spectrum of the femtosecond pulse may overcome the lack of energy through an effect of some higher order process. However, a below band-gap excitation could select the excitation of specific defect-related transitions. The optically induced birefringence in Fig. 1 is one order of magnitude larger than that observed in the experiment of bulk coherent phonons in $SrTiO_3$,[24] and this large value of ellipticity is not expected from a surface effect caused by surface states but is considered to be a bulk effect. In any case, the observed same luminescence spectrum indicates that the same relaxed excited state as that generated by direct ultraviolet excitation, in which localized hole polarons and itinerant electron polarons coexist, is generated in our experiment in the time region of ~100 ps, although the excitation processes and relaxation channels could be different.

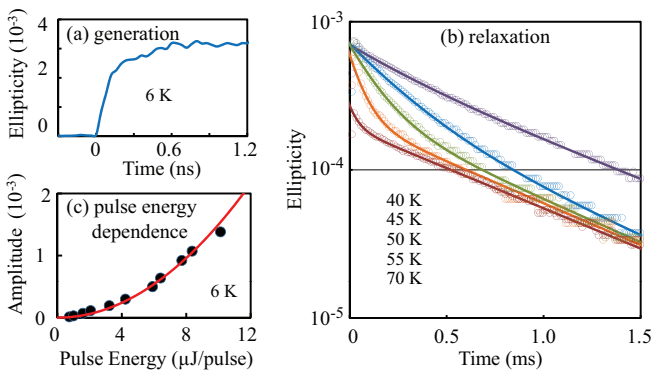

FIG. 1. (Color online) Observed (a) generation and (b) relaxation signals of the lattice distortion after the pulse excitation at $t = 0$. The solid curves in (b) are the fitting curves calculated from the sum of exponentials in Eq. (1). (c) Dependence of the lattice-distortion amplitude on the pump pulse energy. The solid curve in (c) is a fitting curve using square function.

The temperature dependence of the relaxation curve between 40 and 70 K is shown in Fig. 1(b), in which the time resolution of the measurement system is ~10 μs. The relaxation curve $f(t)$ of the lattice-distortion signal can be fitted by the sum of exponentials:

$$f(t) = \sum_i A_i \exp(-\gamma_i t), \tag{1}$$

where A_i and γ_i are the amplitude and relaxation rate of the ith component. The solid curves in Fig. 1(b) show the fitting curves using Eq. (1). At each temperature, the relaxation curve is explained well to have two decay components. In the relaxation analysis, we neglected the fast transients in the time region less than ~0.1 ms. This is because the diffusion of the lattice distortion, which is discussed later, can generate an additional dynamics in that region. The temperature dependence of the relaxation rate obtained from the observed lattice-distortion signal is plotted on a linear scale in Fig. 2(a) and on a logarithmic scale in Fig. 2(b), in which four relaxation components (γ_1, γ_2, γ_3, and γ_4) can be clearly seen. As the temperature increases, the relaxation rates of three components (γ_1, γ_2, and γ_3) show divergence behaviors successively at ~30, ~60, and ~110 K, after which each relaxation component disappears. The transition of the transients shown in Fig. 1(b) indicates the disappearance of the γ_2 component.

The temperature dependence of the relaxation rate $\gamma_i(T)$ ($i = 1,2,3$) for each relaxation component can be fitted by the Arrhenius equation

$$\gamma_i(T) = B_i \exp\left(-\frac{E_i}{T}\right) + C_i, \tag{2}$$

where E_i is the activation energy, k_B is the Boltzmann constant, and B_i and C_i are constants. The solid curves in Figs. 2(a) and 2(b) show the fitting curves calculated from Eq. (2) and explain well the observed relaxation rates. The activation energies obtained from the Arrhenius plots, which correspond to the slope in Fig. 2(b), are $E_1 = 250 \pm 50$ K, $E_2 = 300 \pm 30$ K, and $E_3 = 350 \pm 30$ K for γ_1, γ_2, and γ_3, respectively. The processes characterized by the constants C_i are independent of the temperature and different from the thermal activation processes characterized by B_i and E_i in the first term of Eq. (2). The constants C_i may correspond

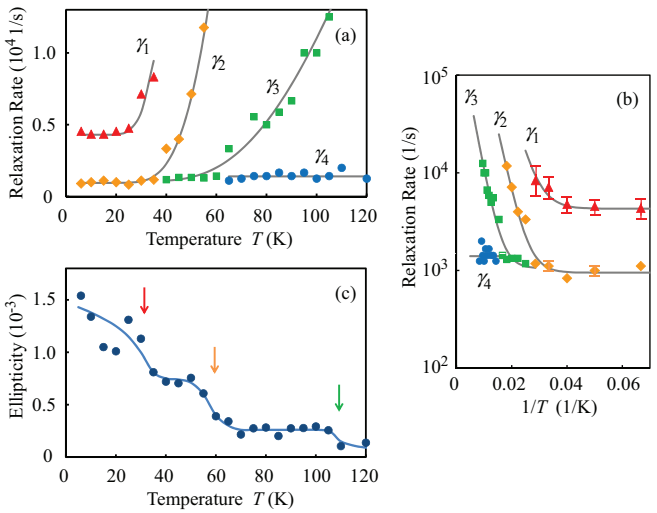

FIG. 2. (Color online) Temperature dependence of the relaxation rate obtained from the observed lattice-distortion signal plotted (a) on a linear scale and (b) on a logarithmic scale. The horizontal axis in (b) is the inverse temperature. The solid curves in (a) and (b) show the fitting curves calculated from the Arrhenius equation in Eq. (2). (c) Temperature dependence of the observed lattice-distortion amplitude. The solid curve in (c) serves as a visual guide.

to quantum mechanically determined lifetimes of the lattice distortions. However, the details of the physical origins are not known at present.

The temperature dependence of the observed lattice-distortion amplitude is shown in Fig. 2(c). As the temperature increases, the lattice-distortion amplitude shows steplike decreases at ∼30, ∼60, and ∼110 K. This result is consistent with the divergence behavior of the relaxation rate at each of these temperatures. These experimental results can be interpreted by successive thermal quenching of three kinds of lattice distortions. Each amplitude A_i of the relaxation component has a constant value and only the relaxation rate γ_i changes, while in the experiment the amplitude changes continuously because of the finite time resolution. Under this interpretation, the observed amplitudes of the relaxation components are $A_1 = (5.0 \pm 0.8) \times 10^{-4}$, $A_2 = (4.6 \pm 0.2) \times 10^{-4}$, $A_3 = (1.4 \pm 0.2) \times 10^{-4}$, and $A_4 = (1.2 \pm 0.2) \times 10^{-4}$.

The experimental results in the above suggest that the lattice distortions are caused by the photogenerated carriers in at least three kinds of trapped states and are thermally quenched successively as the temperature increases. The photogenerated carriers may be trapped by intrinsic crystal defects around oxygen vacancies. One of the candidates for hole-trapping centers is the Ti^{3+} ion in Ti^{3+}-oxygen vacancy complexes.[25] Since electrical conduction due to holes is not observed, most of the photogenerated holes may be deeply trapped at Ti^{3+} sites of the complexes. Conversely, the photogenerated electrons are considered to be itinerant, and luminescence arises from the recombination of the shallowly trapped electrons with the holes localized around the defects. The divergence in the relaxation rate at ∼30 K is considered to have the same origin with the decreasing intensity of the green luminescence (∼2.4 eV) above ∼30 K,[9,13,14,25] after which the carriers trapped in localized states vanish via a thermal activation process before radiative recombination. The divergence at ∼110 K is considered to be due to the structural phase transition at 105 K, at which a tetragonal distortion from the high-temperature perovskite cubic structure occurs. This deformation can be pictured as alternate librations of TiO_6 octahedra, and three kinds of domains with three directions of the tetragonal axis along the [100] axis exist in the crystal. The disappearance of this structural deformation is considered to change the local defect dynamics. The divergence at ∼60 K may be related to the thermal quenching of photocurrent above ∼60 K (Ref. 9) or the dielectric anisotropy found below ∼60 K.[26] The relaxation signals in the above arise from localized lattice distortions. These distortions generate birefringence along the [100] axis, and their amplitudes are characterized by A_i and γ_i in Eq. (1). However, the details of each local structure and dynamics is not known at present.

IV. SPATIAL DIFFUSION OF THE LATTICE DISTORTION

We observed the lattice-distortion signal induced by a separated pump beam from the probe beam to investigate its itineracy. The dependence of the optically induced lattice-distortion signal on the separation observed at 25 K is shown in Fig. 3(a), where the separation between the pump and probe beams is 0.2, 0.3, 0.4, and 0.5 mm along the [100] axis. The two beams on the sample are monitored by a complementary metal-oxide semiconductor image sensor, and the position of the pump beam is adjusted by changing the angle of a bending mirror. As the separation becomes larger, the signal becomes smaller around $t = 0$ and rises later. This is because the overlap between the pump and probe beams becomes smaller and the pumped part in the probed area becomes smaller. The signal appears later as the separation between the pump and probe beams becomes larger. This result indicates that the optically induced lattice distortion generated in the pumped area diffuses and reaches to the probed area after spatial migration.

We also attempted to observe the diffusion of the lattice distortion along the [110] axis. The lattice distortion signals for small values of separation are shown in Fig. 4. The relaxation signal disappears as the overlap between the pump and probe beams becomes smaller. In the case along the [100] axis

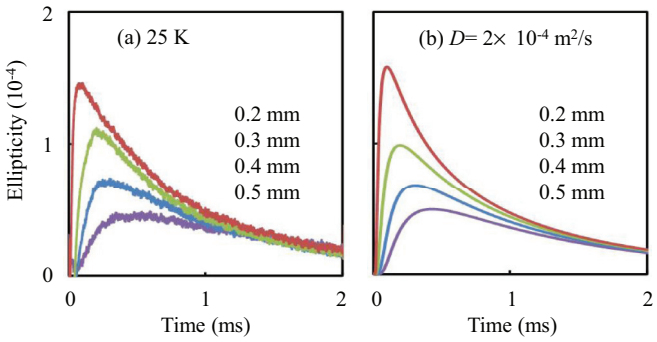

FIG. 3. (Color online) (a) Lattice distortion signals induced by a separated pump beam from the probe beam, observed at 25 K. The separation between the pump and probe beams is 0.2, 0.3, 0.4, and 0.5 mm along the [100] axis. (b) Simulation curves using the solution of the diffusion equation for a point source in Eq. (4) with $d = 1$ and $D = 2 \times 10^{-4}$ m^2/s.

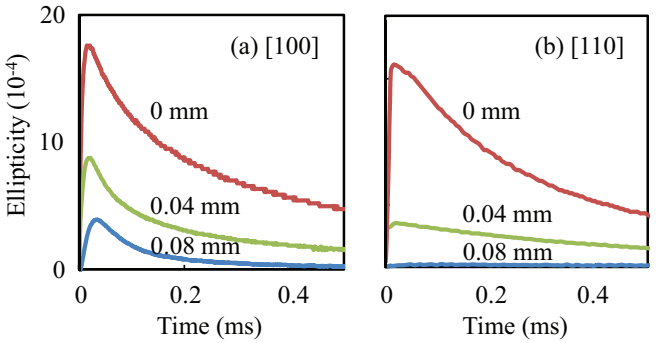

FIG. 4. (Color online) Lattice distortion signals induced by a separated pump beam from the probe beam, observed at 6 K. The separation between the pump and probe beams is 0, 0.04, and 0.08 mm (a) along the [100] axis and (b) along the [110] axis.

in Fig. 4(a), the diffusion signal remains in the short-time region. However, in the case along the [110] axis in Fig. 4(b), no signal remains. This result indicates that the optically induced lattice distortion diffuses only along the [100] axis. The lattice-distortion signals for 0-mm separation in Figs. 4(a) and 4(b) are expected to be the same. However, the signal curves in the short-time region are not the same. This may be caused by the difference in the accuracy of the beam overlap and/or the deviation of the beam cross-section shape from a circle to an ellipse. The adjustment of beam position with accuracy less than 0.01 mm is not easy, and the diffusion signal for small separations is sensitive to the direction of misadjustment and the intensity distributions in the beam cross sections.

The diffusion signals of the lattice distortion for the separations of 0.2 and 0.3 mm observed at 6 and 30 K are shown in Fig. 5. As the temperature increases, the signal peak appears later. This indicates that the spatial diffusion of the lattice distortion becomes slower at higher temperatures.

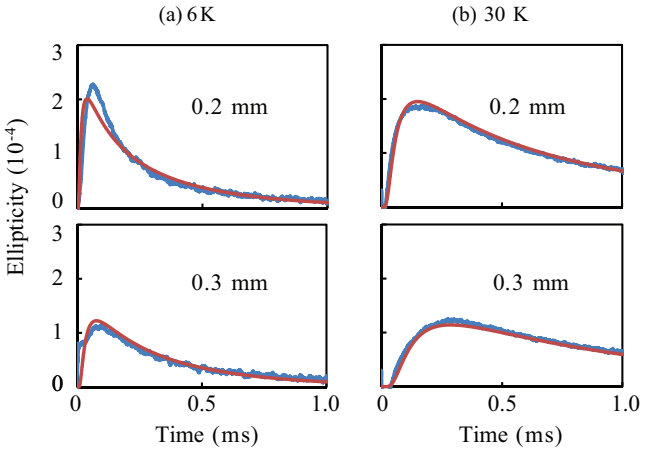

FIG. 5. (Color online) Diffusion signals of the lattice distortion for separations of 0.2 and 0.3 mm between the pump and probe beams, observed at (a) 6 and (b) 30 K. The solid curves show the simulation curves using the solution of the diffusion equation for a point source in Eq. (4) with $d = 1$.

The diffusion dynamics of a physical quantity $n(r,t)$ is described by the diffusion equation

$$\frac{\partial n(\boldsymbol{r},t)}{\partial t} = D\nabla^2 n(\boldsymbol{r},t), \tag{3}$$

where D is the diffusion coefficient. The solution of the diffusion equation for a point source at $\boldsymbol{r} = \boldsymbol{0}$ and $t = 0$ is represented by

$$n(\boldsymbol{r},t) = \left(\frac{1}{4\pi Dt}\right)^{d/2} \exp\left(-\frac{r^2}{4Dt}\right), \tag{4}$$

where d is the dimension of the space.

We simulated the observed diffusion signals using the solution of the diffusion equation for a point source in Eq. (4) and obtained the value of diffusion coefficient D in the one-dimensional case ($d = 1$). The solid curves in Figs. 3(b) and 5 show the simulation curves, and the observed diffusion curves are reproduced well. The values of the diffusion coefficient D obtained from the simulation are $(5.0 \pm 1.5) \times 10^{-4}$ m^2/s (6 K), $(1.9 \pm 0.5) \times 10^{-4}$ m^2/s (25 K), and $(1.1 \pm 0.3) \times 10^{-4}$ m^2/s (30 K). In the simulation, a relaxation factor $\exp(-\gamma t)$ is added to Eq. (4), where $\gamma \approx 10^3$ s^{-1} is the relaxation rate. This factor is used to fit the long tail of the signal up to 4 ms. The behavior of the signal peak is important to determine the diffusion coefficient, but the peak time is not sensitive to the relaxation rate. This relaxation arises from the itinerant lattice distortion and is different from that shown in Fig. 2, which arises from the localized lattice distortions.

The two-photon absorption efficiency is proportional to the square of the pump intensity. Therefore, the relaxed excited state is generated more efficiently at the center of the beam spot. If we assume the two-photon absorption and a simple Gaussian intensity profile with a diameter of 50 μm, the effective diameter of the generation is expected to be $\sim$35 μm. In the simulation, we used a point-source approximation and did not take the finite spot size into consideration. For the separation less than 0.2 mm and large diffusion coefficient, the simulation does not work well. However, it works well for the separation of more than 0.2 mm as shown in Figs. 3 and 5, in which the separation is almost one order of magnitude larger than the pump spot size. For the 0.2-mm separation in Fig. 5(a), the deviation of the simulation curve from the observed curve is not small. This is because the point-source approximation is not valid for the short-time diffusion dynamics in the case of small separation and large diffusion coefficient.

In two- and three-dimensional simulations, the peak amplitude decreases rapidly as the separation increases, and the observed amplitude cannot be reproduced. One-dimensional simulation works best, which is consistent with the no diffusion signal along the [110] axis in the experiment.

The Hall mobility of the photogenerated electrons obtained from the photo-Hall measurements[11,12] is $\sim 10^4$ cm^2/V s at 5 K. The mobility μ of the lattice distortion can be derived from the diffusion coefficient D using the Einstein relation

$$eD = \mu k_B T. \tag{5}$$

The mobility of the lattice distortion derived from the observed diffusion coefficient in our experiment is shown in Fig. 6. The temperature dependence of this mobility is qualitatively

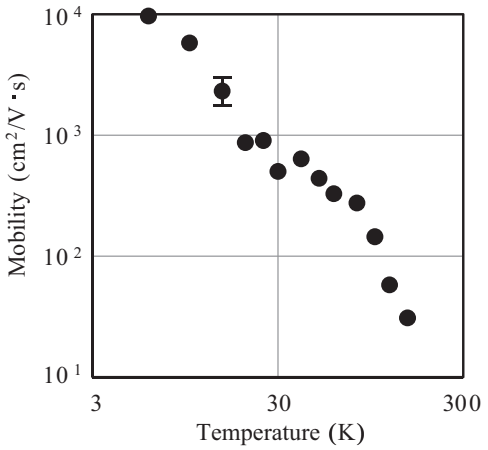

FIG. 6. Temperature dependence of the mobility of the lattice distortion in $SrTiO_3$ derived from the observed diffusion coefficient in our experiment using the Einstein relation.

consistent with that of the Hall mobility of the photogenerated electrons.[11,12] This result strongly suggests that the origin of the diffusive lattice distortion is the photogenerated polarons, which are electrons accompanied by lattice distortion in the relaxed excited state.

According to the theory of superparaelectric large polaron,[19] the enhancements of electronic conductivity and quasistatic electric susceptibility can be explained if the photogenerated electrons, being quite itinerant in the $3d$ band of the Ti^{4+} ion, are assumed to couple weakly but quadratically with soft anharmonic T_{1u} phonons. The deformation direction of the T_{1u} mode in the perovskite structure is along the [100] axis, which is consistent with the direction of the birefringence observed in our experiment. This deformation direction may also determine the observed diffusion direction only along the [100] axis. The spatial and temporal dynamics of polaron diffusion have been observed directly in our experiment. The diffusive carriers are considered to be intrinsic and itinerant electron polarons, whereas the relaxation of the lattice distortion in Fig. 2 is caused by localized polarons, or photogenerated carriers trapped in localized centers.

V. SUMMARY

In conclusion, the lattice dynamics of the relaxed excited state in an incipient ferroelectrics $SrTiO_3$ was studied by using the pump-probe technique. Successive thermal quenching of three kinds of lattice distortions was observed in the relaxed excited state. As the temperature increases, the three relaxation components show divergence behaviors of the relaxation rate and steplike decreases in the amplitude owing to the successive disappearance of the relaxation components. These processes are considered to be caused by localized polarons, which are photogenerated carriers in trapped states and play important roles in photoluminescence or photoconductivity. The evidence for the spatial diffusion of the lattice distortion along the [100] axis was shown in the experiment using the separated pump beam from the probe beam. The optically induced lattice distortion was found to diffuse only along the [100] axis. The diffusion coefficient was obtained from the simulation of the observed diffusion signals using the solution of the diffusion equation. The temperature dependence of the mobility of the lattice distortion obtained from the observed diffusion coefficient is qualitatively consistent with the Hall mobility of the photogenerated electrons. This suggests that the origin of the diffusive lattice distortion is itinerant electron polarons, which are electrons accompanied by a lattice distortion. A direct observation of the spatial and temporal dynamics of polaron diffusion has been demonstrated by our experiment.

[1]H. Fröhrich, Adv. Phys. **3**, 325 (1954).
[2]*Polarons and Excitons*, edited by C. G. Kuper and G. D. Whitfield (Oliver and Boyd, Edinburgh-London, 1963).
[3]S. Sasamoto, J. Hirohashi, and S. Ashihara, J. Appl. Phys. **105**, 083102 (2009).
[4]R. P. Prasankumar, S. Zvyagin, K. V. Kamenev, G. Balakrishnan, D. M. Paul, A. J. Taylor, and R. D. Averitt, Phys. Rev. B **76**, 020402(R) (2007).
[5]C. Soci, D. Moses, Q.-H. Xu, and A. J. Heeger, Phys. Rev. B **72**, 245204 (2005).
[6]G. Allodi, M. C. Guidi, R. De Renzi, A. Caneiro, and L. Pinsard, Phys. Rev. Lett. **87**, 127206 (2001).
[7]H. Matsui, T. Hasegawa, Y. Tokura, M. Hiraoka, and T. Yamada, Phys. Rev. Lett. **100**, 126601 (2008).
[8]K. A. Müller and H. Burkard, Phys. Rev. B **19**, 3593 (1979).
[9]T. Feng, Phys. Rev. B **25**, 627 (1982).
[10]H. Katsu, H. Tanaka, and T. Kawai, Jpn. J. Appl. Phys. **39**, 2657 (2000).
[11]H. Yasunaga, J. Phys. Soc. Jpn. **24**, 1035 (1968).
[12]T. Ishikawa, M. Kurita, H. Shimoda, Y. Sakano, S. Koshihara, M. Itoh, and M. Takesada, J. Phys. Soc. Jpn. **73**, 1635 (2004).
[13]R. Leonelli and J. L. Brebner, Phys. Rev. B **33**, 8649 (1986).
[14]T. Hasegawa, M. Shirai, and K. Tanaka, J. Lumin. **87–89**, 1217 (2000).
[15]T. Hasegawa and K. Tanaka, J. Lumin. **94-95**, 15 (2001).
[16]M. Takesada, T. Yagi, M. Itoh, and S. Koshihara, J. Phys. Soc. Jpn. **72**, 37 (2003).
[17]T. Hasegawa, S. Mouri, Y. Yamada, and K. Tanaka, J. Phys. Soc. Jpn. **72**, 41 (2003).
[18]Y. Qiu and K. Nasu, J. Lumin. **112**, 271 (2005).
[19]K. Nasu, Phys. Rev. B **67**, 174111 (2003).
[20]L. Sponza, V. Véniard, F. Sottile, C. Giorgetti, and L. Reining, Phys. Rev. B **87**, 235102 (2013).
[21]T. Kohmoto, Y. Fukuda, M. Kunitomo, and K. Isoda, Phys. Rev. B **62**, 579 (2000).
[22]T. Kohmoto, Y. Koyama, T. Moriyasu, H. Okamura, Y. Yamada, and K. Tanaka, J. Phys. Soc. Jpn. **80**, 104605 (2011).
[23]T. Kohmoto, D. Ikeda, X. Liang, and T. Moriyasu, Phys. Status Solidi C **9**, 2582 (2012).
[24]T. Kohmoto, K. Tada, T. Moriyasu, and Y. Fukuda, Phys. Rev. B **74**, 064303 (2006).
[25]S. Mochizuki, F. Fujishiro, and S. Minami, J. Phys.: Condens. Matter **17**, 923 (2005).
[26]T. Sakudo and H. Unoki, Phys. Rev. Lett. **26**, 851 (1971).